Nanoscopic Lipid Domain Dynamics Revealed by Atomic Force Microscopy

Fuyuki Tokumasu,* Albert J. Jin,† Gerald W. Feigenson,‡ and James A. Dvorak*
*Laboratory of Malaria and Vector Research, National Institute of Allergy and Infectious Diseases, †Division of Bioengineering and Physical Science, Office of Research Service, Office of Director, National Institutes of Health, Bethesda, Maryland 20892; and ‡Department of Molecular Biology and Genetics, Cornell University, Ithaca, New York 14853

ABSTRACT Intrinsic heterogeneities, represented as domain formations in biological membranes, are important to both the structure and function of the membranes. We observed domain formations in mixed lipid bilayers of dipalmitoylphosphatidylcholine (DPPC), dilauroylphosphatidylcholine (DLPC), and cholesterol (chol) in a fluid environment using an atomic force microscope (AFM). At room temperature, we demonstrated that both microscopic and nanoscopic domains coexist and the DPPC-rich domain is ~1.4 nm higher than the surrounding DLPC-rich membrane areas as a consequence of intrinsic phase differences. DPPC-rich microscopic domains became larger as DPPC concentration increased. In cholesterol-free mixtures, nanoscopic DPPC-rich domain sizes ranged from 26 to 46 nm depending on phospholipid concentration. Domain size varied between 33 and 48 nm in the presence of cholesterol ($0 \leq [chol] \leq 40$). The nanoscopic domains were markedly fragmented near $[chol] = 0.135$ and appeared to fuse more readily into microscopic domains at higher and lower [chol]. By phase balance analyses we demonstrated phase behavior differences between a free-vesicle GUV system studied by confocal light microscopy and a supported membrane system studied by AFM. We propose a new three-dimensional phase diagram elucidating the effects of a solid substrate support on lipid phase behavior relevant to complex membrane phase phenomena in biological systems.

INTRODUCTION

Biological membrane heterogeneities are responsible for processes as diverse as the formation of membrane domains with or without lipid phase separations. One subset of biological membrane heterogeneities termed detergent-resistant membranes (DRMs) or rafts (Anderson and Jacobson, 2002; Simons and Ikonen, 1997), are characterized by their resistance to cold, nonionic detergents such as Triton X-100. These rafts are involved in biological processes such as membrane fusion, signal transduction, and virus release at the cell membrane level (Lang et al., 2001; Ono and Freed, 2001; Sheets et al., 1999; Stefanova et al., 1991). Biochemical studies demonstrate that membrane rafts are rich in sphingolipids, phospholipids, and cholesterol, as well as glycophosphatidylinositol (GPI)-anchored and other proteins. At physiological temperatures it has been proposed that rafts are liquid-ordered phase domains (cf. Brown and London, 2000). Although data from detergent solubility studies confirm the existence of rafts and their modifications by intrinsic and extrinsic factors, the mechanisms involved in raft formation, behavior, and structure remain to be elucidated.

Mixed lipid bilayers are excellent model systems for lipid distributions involved in membrane rafts. Well-defined mixtures can provide physical chemical insights relevant to native biological membrane systems. Supported lipid bilayers and giant lipid vesicles assayed by techniques such as fluorescence microscopy (Dietrich et al., 2001; Hwang et al., 1995) and x-ray and neutron diffraction (Bedzyk et al., 1988; Koenig et al., 1996) have been used to both visualize and elucidate lipid phase behavior and phase separations. Although lateral phase separations are detectable by these techniques, many structural characteristics of phase domains remain to be elucidated. Recently, atomic force microscopy (AFM) has been used to study lipid mixtures, in the form of vesicles and membranes, and biological structures at very high spatial resolution with minimal sample manipulation or preparation. AFM has been used to directly visualize living cell membranes and submembraneous structures (Braet et al., 1998; Nagao and Dvorak, 1998; Henderson et al., 1992; Swihart et al., 2001; Ushiki et al., 1999), membrane protein structures (Kaasgaard et al., 2002; Muller et al., 2000; Takeyasu et al., 1996) as well as the domain structures of cell membranes (Giocondi et al., 2000) and mixed lipid membranes (cf. Dufrene et al., 1998 and Tokumasu et al., 2002).

We report here an AFM study of the phase properties of domains using three component mixed lipid bilayers composed of 1,2-dipalmitoyl-*sn*-glycero-3-phosphocholine (DPPC), 1,2-dilauroyl-*sn*-glycero-3-phosphocholine (DLPC), and cholesterol (chol), whose overall phase behavior as giant unilamellar vesicles (GUVs) was previously studied by confocal fluorescence microscopy (CFM) (Feigenson and Buboltz, 2001). The GUV study demonstrated a relationship between phase behavior and domain separation at a resolution of ~400 nm. In addition, using fluorescence resonance energy transfer (FRET) (Feigenson and Buboltz, 2001) proposed that nanoscopic domains may exist where domain separation could not be resolved by conventional CFM. Here we report the coexistence of microscopic and nanoscopic domains and quantitative analyses of nanoscopic

Submitted June 14, 2002, and accepted for publication December 2, 2002.

Address reprint requests to James Dvorak, Email: jdvorak@niaid.nih.gov.

0006-3495/03/04/2609/10 $2.00

domains, as small as ~25 nm. We also describe the dependence of microscopic domain size on cholesterol concentration and a theoretical treatment of phase balance of supported lipid bilayers that amplifies the previous report on GUVs. Our results provide new insights into membrane physical chemistry relevant to cell membranes in a native environment.

MATERIALS AND METHODS

Materials

Phospholipids were obtained from Avanti Polar Lipids, Inc. (Alabaster, AL) and cholesterol was purchased from Nu Chek Prep (Elysian, MN). Purity of >99.5% was confirmed by thin-layer chromatography on washed, activated silica gel plates (Alltech, Deerfield, IL) developed with chloroform/methanol/water (65:25:4) for both phospholipids and with petroleum ether/diethyl ether/chloroform (7:3:3) for cholesterol. Phospholipid stock solutions were quantified by phosphate assay (Kingsley and Feigenson, 1979).

Vesicle and supported lipid membrane preparation

Multilamellar lipid dispersions were prepared by rapid solvent exchange, essentially as described by Buboltz and Feigenson (1999), but with a somewhat simplified procedure. Phospholipids and cholesterol were dissolved in 50–100 μl chloroform at concentrations of 50–100 nmol and placed in 13 × 100 mm screw-cap culture tubes. PIPES buffer (5 mM PIPES, 200 mM KCl, and 1 mM EDTA, pH = 7.0), 0.5–1 ml was added, and a vacuum of ~23 torr was applied to the tubes for 10 min while vortexing to remove the organic solvent. The tubes were sealed under argon, heated to 50°C for 2 h, and slowly cooled to 23°C over a 12 to 20 h period.

Large unilamellar vesicles (LUVs) were prepared from the multilamellar vesicles with a mini-extruder (Avanti) containing two layers of 100 nm-pore size Nucleopore polycarbonate membranes (Corning, Corning, NY). Extrusions were performed for 50 cycles in the same PIPES buffer at 49°C, a temperature at which both phospholipids are in the fluid phase. The size homogeneity of vesicles prepared by this method has been described (Jin et al., 1999; Pencer et al., 2001). After extrusion, the vesicle suspensions were placed in an 8400 cm^3-styrofoam box (wall thickness ~5 cm) containing ~3.5 L of ~50°C water and allowed to equilibrate overnight to room temperature.

Supported membrane bilayers were prepared from LUV suspensions as described previously (Tokumasu et al., 2002). In brief, a 5 μl portion of a freshly prepared LUV suspension was applied onto freshly cleaved mica, incubated for 30 s and washed with the PIPES buffer. Excess fluid was removed and the sample was placed in a liquid cell attached to a Multimode AFM (Digital Instruments, Santa Barbara, CA). The sample was equilibrated in the same extrusion buffer for 20–30 min before imaging. We used the liposome adsorption method instead of the alternative Langmuir-Blodgett (LB) surface film deposition method (see e.g., Diociaiuti et al., 2002), to prepare supported membranes of various three-component mixtures. The liposome adsorption technique is more reliable for easier establishment, maintenance, and control of a known lipid mixture ratios and symmetry between the two leaflets in the resulting surface bilayers. In contrast, the LB method is better for the preparation of supported monolayers and for making bilayers that are asymmetric between two leaflets.

Atomic force microscopy

Imaging was performed using tapping mode at room temperature at a scanning rate of 1.5 Hz with a Multimode AFM and a Nanoscope IIIa controller (Digital Instruments), a Type D scanner (max scanning range: 10 μm × 10 μm) and silicon nitride DNP probes (Digital Instruments), having a nominal spring constant of 0.58 N/m. A controlled environment chamber was used to minimize perturbations from the temperature increase of the piezo scanner that normally occurs during imaging (Tokumasu et al., 2002). The tapping frequency was ~8.7 kHz. Soft tapping was maintained by keeping the ratio of cantilever oscillation amplitudes before and after probe engagement of the sample surface (A_{sp}/A_0) at ~8.8 (Magonov et al., 1997). Images were acquired and stored in either 512 × 512 or 512 × 256 pixel-element formats and converted to uncompressed linear 8-bit gray scale TIF format for further analyses. Domain size measurements were made using Image Pro Plus version 4.5 (Media Cybernetics, Silver Spring, MD) and numeric data were exported to Microsoft Excel for modeling and statistical analyses. Statistical analyses of domain size distributions and phase balance analyses were carried out using Origin version 5.0 (OriginLab, Northampton, MA) and Mathcad version 8.0 (Mathsoft, Cambridge, MA), respectively. Probe-tip size estimates were performed as described (Bustamante and Keller, 1995) using tobacco mosaic virus (TMV). The membrane domain size was calculated with a correction for tip-induced broadening using a step-height sample model (Takeyasu et al., 1996).

RESULTS

Mixed lipid bilayers form domains

The coexistence of a microscopic DPPC-rich ordered gel phase and a DLPC-rich disordered liquid-crystalline phase in GUV membranes have been demonstrated by confocal fluorescence microscopy (CFM) and fluorescence resonance energy transfer (FRET) measurements (Feigenson and Buboltz, 2001). Although CFM data showed micrometer-size phase separations, nanoscopic domains were not detected as they are below the lateral resolution limit of the CFM. However, FRET analyses implied that three-component lipid mixtures can form nanoscopic domains at certain mixture ratios (Feigenson and Buboltz, 2001). Therefore, we studied by AFM these specific mixture ratios to determine if nanoscopic domain structures could be identified.

We use two parameters to describe sample composition, χ_{DPPC} (the mole fraction of DPPC of all phosphatidylcholines: PC) and χ_{chol} (the mole fraction of cholesterol in the total mixture). Fig. 1 shows AFM images of a DLPC/DPPC/chol ($\chi_{DPPC} = 0.7$ and $\chi_{chol} = 0.189$) mixed lipid bilayer with structural domains. This lipid concentration is near the center of region D described by Feigenson and Buboltz (2001) where free GUV membrane is thought to contain only nanoscopic, but not microscopic, domains. Here we observed both nanoscopic domains and some intermediate size domains (100 nm < diameter < 1 μm). The domains were distributed over the entire membrane surface and showed a heterogeneous size distribution with the intermediate size domains predominating at the edges of the membrane patches. In contrast, nanoscopic domains, with an apparent size of ~50 nm, showed a more random distribution than larger domains. The contours of the larger domains are rough and have a more irregular shape. Similar domain border structures have been reported (Milhiet et al., 2001; Sikes and Schwartz, 1997; Yuan and Johnston, 2001). Analyses of membrane

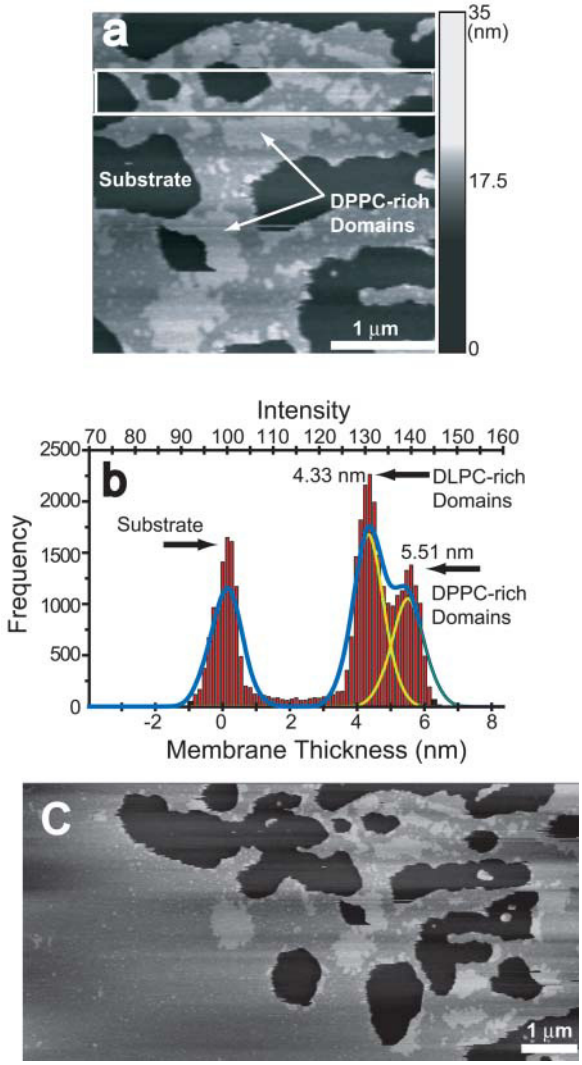

FIGURE 1 Domain formation in a multi-component lipid mixture. (*a*) Representative example of membrane domains formed by a DLPC:DPPC = 3:7, $\chi_{chol} = 0.185$ mixture at room temperature. Bright and dark membrane regions represent DPPC-rich and DLPC-rich domains, respectively. Note that both micro- and nanoscopic domains coexist throughout the membrane. (*b*) Height analysis of membrane thickness measured in the rectangular box shown in *a*, selected so that three height components are clearly shown. A multi-peak Gaussian model was used to identify the substrate, lower, and higher domains on the basis of diffuse optical density differences. The lipid membrane heights were estimated relative to the substrate peak set to zero. (*c*) Larger image (5 μm $\times$10 μm) of *a* showing higher membrane coverage. The larger domains preferentially formed at edges are clearly shown. The full height gray scale is 35 nm for both *a* and *c*; and the *x*-*y* scales are denoted by the 1 μm bars. The supported bilayer for this lipid composition is in the region D of the free GUV phase diagram (Fig. 6) where nanoscopic domains were predicted.

height profiles revealed two Gaussian distributions with peaks at ~4.3 nm and ~5.5 nm, representing DLPC-rich and DPPC-rich domain regions, respectively (Fig. 1 *b*). The interdomain difference in membrane thickness was ~1.2 nm, consistent for both nanoscopic domains and submicrometer size domains. These thickness measurements are in good agreement with both x-ray diffraction and neutron diffraction data on pure DPPC (~6.0 nm) and DLPC (~4.2 nm) membranes (Balgavy et al., 2001; Nagle and Tristram-Nagle, 2000; Cevc and Marsh, 1987). In high coverage areas, membranes clearly showed both nanoscopic as well as submicrometer size domains (Fig. 1 *c*). Nanoscopic domain size appears to be similar in large patches or in nearly intact single bilayers; larger domain size is not restricted by the size of the membrane patch that typically reached our AFM scan size limit of 5 $\times$ 10 μm. Our AFM data demonstrate that in addition to the microscopic domains visible in CFM, nanoscopic domains do indeed exist below the resolution limit of CFM and can be observed directly by AFM.

DLPC and DPPC mixtures

The previous study of GUVs (Feigenson and Buboltz, 2001) demonstrated that phase separation patterns varied depending on the DPPC/DLPC/chol mixture ratios. They also showed that no CFM-observable phase separation occurred at certain lipid mixture ratios (cf. Fig. 2 *d*) as expected. We imaged multiple samples with different lipid compositions both with and without cholesterol to determine how domain formation is controlled by lipid mixture ratio. AFM images (Fig. 2) in cholesterol-free conditions ($\chi_{DPPC} = 0.2, 0.5, 0.8$), show a mixed architecture of nanoscopic and microscopic domains, similar to CFM images at equivalent DPPC concentrations. At low χ_{DPPC}, large DPPC-rich domains were observed only at the edges of the membrane whereas small nanoscale domains were present throughout the surrounding membrane areas (Fig. 2 *a*). In contrast, CFM images showed a homogeneous distribution of DLPC and the distributions of the two phospholipids were uniformly intermixed (Fig. 2 *d*). When χ_{DPPC} was increased to 0.5 (Fig. 2 *b*), a larger number of predominately DLPC-rich areas were still observed. In contrast to CFM images where a DLPC-rich phase occupied larger areas (Fig. 2 *e*), AFM demonstrated that domains existed not only at membrane edges but also within membrane regions. More nanoscopic domains appeared although significant growth of larger DPPC-rich domains was not observed. In addition, weaker attachment of the membrane to the mica substrate was noticed during sample preparation. These data imply that the phase behavior changed. At $\chi_{DPPC} = 0.8$, significantly more microscopic membrane domains were seen by AFM (Fig. 2 *c*), and nanoscopic domains with diameters of ~46 nm were still dispersed throughout all membrane areas. We were unable to identify domain-like structures in either DLPC or DPPC single-lipid samples at room temperature (data not shown). Therefore, as in free GUV membranes, phase coexistence occurs for a range of χ_{DPPC}. However, CFM images show that a DPPC-rich phase region occupies a larger fraction of the membrane area than was seen by AFM at all corresponding DLPC/DPCP mixtures. These data fortify the concept that supported membranes contain both nanoscopic

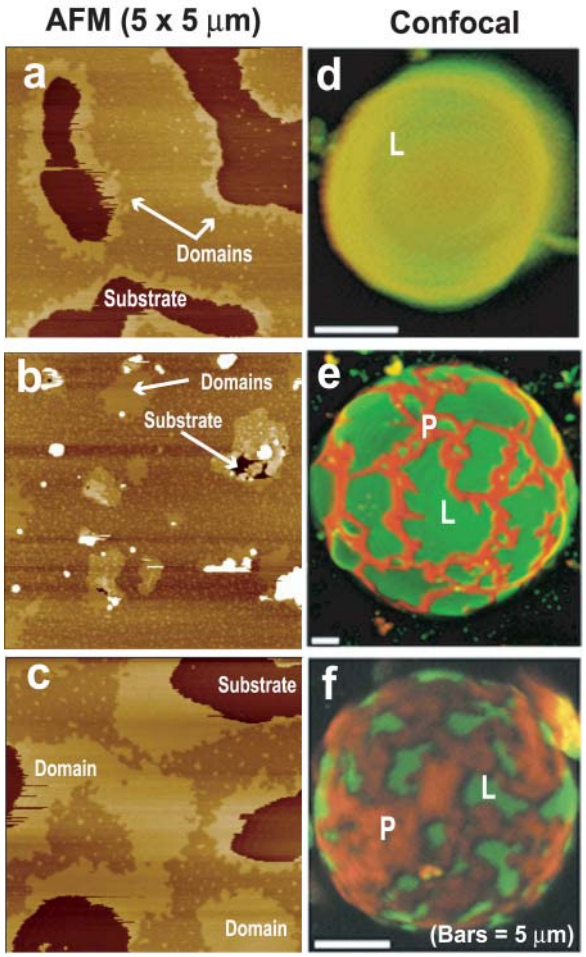

FIGURE 2 Comparisons of domain formations seen by AFM and CFM at $\chi_{chol} = 0$. (*a*) At 20% DPPC: 80% of DLPC, microscopic domains formed only at the edges of the membrane. (*b*) A membrane containing 50% DPPC showed a slight increase in domain area. (*c*) At 80% DPPC, the area occupied by DPPC-rich domains markedly increased. (*d*) A CFM image corresponding to at $\chi_{DPPC} = 0.2$ did not show any domains; the distribution of the two lipids molecules appeared to be homogeneous. (*e*) In contrast to the AFM image in *b*, the CFM image at $\chi_{DPPC} = 0.5$ showed a clear phase separation with a larger DLPC-rich phase (~70%, represented as L) than a DPPC-rich phase (~30%, represented as P). However, the DLPC-rich phase is still continuous. (*f*) The CFM image at $\chi_{DPPC} = 0.8$ showed that the DPPC-rich phase has become larger (~80%) and more continuous. The membrane coverage in *a–c* is of a partial bilayer to nearly a perfect bilayer and scale bars for *d*, *e*, and *f* are 5 μm.

and microscopic domains, but exhibit phase behaviors quantitatively different than unsupported GUVs. In all cases, higher membrane domains present a flat surface and none of our AFM samples showed nanoscopic DLPC-rich domains contained within larger DPPC-rich structures.

Phospholipid and cholesterol mixtures

AFM images of phospholipid-chol mixtures showed domain structures that are markedly influenced by the cholesterol concentration (Fig. 3). At $\chi_{chol} = 0$ and $\chi_{DPPC} = 0.6$, large

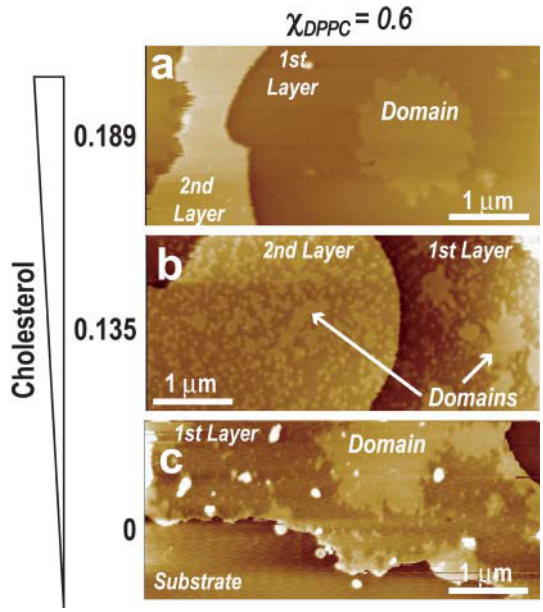

FIGURE 3 Cholesterol changes microscopic domain size. (*c*) Microscopic domains occupied ~50% of a cholesterol free membrane; (*b*) domains disrupted into smaller units of less than 1 μm ($\chi_{chol} = 0.135$). (*a*) When $\chi_{chol} = 0.189$, medium size domains disappeared and micrometer-size domains and small nanoscopic domains reappeared. These data suggest that the membrane is not in a first-order transitional state at $\chi_{chol} = 0.135$ and the nanoscopic domains predominate. Membrane coverage exceeded one full bilayer in *a* and *b*. The difference between domain appearance in the first and second membrane bilayer may reflect the differences in support from the mica surface.

domains with micrometer size diameters occupied ~50% of the membrane area (Fig. 3 *c*). However, at $\chi_{chol} = 0.135$ and $\chi_{DPPC} = 0.6$, the large domains dissociated into small domains with diameters of ~46 nm and into medium size clusters with diameters of several hundreds of nm; no domains with diameter larger than ~1 μm were found (Fig. 3 *b*). This fragmentation of nanoscopic domains is especially clear in the second membrane layer over the mica surface (Fig. 3 *b*). When χ_{chol} was increased to 0.185, small domains with diameters of ~43 nm still existed and a few microscopic domains could be seen (Fig. 3 *a*). These data imply that micrometer-size domain structures at $\chi_{chol} = 0$ were disrupted by the addition of cholesterol and that the membrane was in a transitional state near $\chi_{chol} = 0.135$. Consequently, we predict that there may be a diffuse intermediate region near $\chi_{chol} = 0.135$ along a line of $\chi_{DPPC} = 0.6$, corresponding to the region D reported by Feigenson and Buboltz (2001) . The domain structures at $\chi_{chol} = 0.135$ observed by AFM would appear homogeneous at the resolution limits of CFM. A similar domain pattern over χ_{chol} was also observed along the line of $\chi_{DPPC} = 0.7$ (cf. Fig. 1).

Quantitative analyses of nanoscopic domains

To elucidate the relationship between lipid mixture ratio and

domain formation, we quantified nanoscopic domain size distributions. Various domain sizes varying from nanometers to micrometers were observed. However, as the larger domains have been analyzed by CFM, we concentrated on the smaller domains (≤100 nm) revealed by AFM. This approach allowed us to clarify the structural characteristics of the fundamental domain units which give rise to macroscopic domains.

We used a multi-peak Gaussian model to obtain the peak domain sizes for each distribution (Table 1). All domain size data were corrected for broadening in lateral dimensions due to AFM tip geometry (See Materials and Methods). The average domain size was 42.4 ± 3.5 nm with the exception of $\chi_{DPPC} = 0.5$, where peak domain size was 25.8 ± 0.6 nm (Fig. 4). The distribution at $\chi_{DPPC} = 0.5$ was relatively large (28.3 ± 1.0 nm), but only 11% of the total fell within the 42.4 ± 3.5 nm range.

Cholesterol-containing samples at two different χ_{chol} (0.135 and 0.189) also showed similar domain sizes (44.6 ± 3.3 nm, Table 1). The change in domain size was small for $\chi_{DPPC} = 0.6$ whereas ~4 nm changes occurred between $\chi_{chol} = 0$, 0.135, and 0.189. In contrast, at $\chi_{DPPC} = 0.7$, the peak domain size increased from the cholesterol-free state by as much as ~10 nm when $\chi_{chol} = 0.135$ and decreased by as much as ~7 nm when $\chi_{chol} = 0.189$. At $\chi_{chol} = 0.4$ and $\chi_{DPPC} = 0.7$, peak domain sizes decreased to ~33 nm (data not shown). These relatively large changes in nanoscopic domain size and the AFM images showing a breakdown in micrometer-size domains near $\chi_{chol} = 0.135$ indicate that at least three different states exist along the $\chi_{DPPC} = 0.6$ and $\chi_{DPPC} = 0.7$ isoclines with respect to cholesterol concentration. Considering the full distribution (Fig. 4), nanoscopic domains for various concentration mixtures show significant overlap in diameters size that are centered between 25 nm and 50 nm.

Phase balance in DPPC/DLPC mixtures

AFM data were used to determine the classical phase coexistence boundaries by quantifying the phase partition

TABLE 1 Quantitative analyses of nanoscopic domain sizes

χ_{DLPC} (%)	χ_{DPPC} (%)	χ_{chol} (%)	Domain size (nm)	+/−	N
90	10	0	39.6	0.44	807
80	20	0	45.7	0.95	614
50	50	0	25.8	0.58	345
40	60	0	42.3	0.47	131
30	70	0	38.4	0.63	374
20	80	0	46.0	2.38	395
40	60	13.5	46.2	0.23	300
30	70	13.5	48.4	0.19	1416
40	60	18.9	42.8	0.60	283
30	70	18.9	41.1	0.52	1191

The nanoscopic domain size for each sample was measured directly and analyzed using a multi-peak Gaussian model. Domain sizes of the fit (±SD).

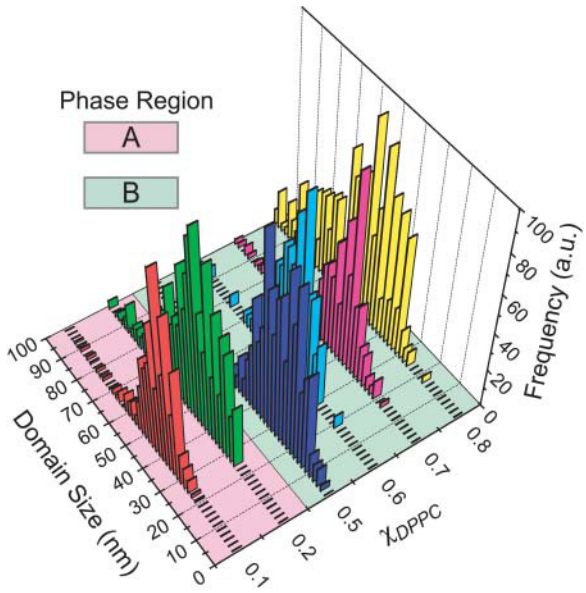

FIGURE 4 Histograms of nanoscopic domain size distributions at $\chi_{chol} = 0$ showing the frequencies of all nanoscopic domains with sizes of less than 100 nm. Domain size at $\chi_{DPPC} = 0.5$ decreased abruptly to ~26 nm from ~46 nm (Table 1) and gradually increased again to ~46 nm. Probable phase regions are shown in pink and green.

between the detected high and low phase areas. For a classical first-order transition with two-phase consistence, a phase balance exists that allows a consistency check of the equilibrium and a determination of the composition of the two phases. For two-phase coexistence between A (DPPC composition x) and B (DPPC composition y), we express the fraction of phase A, FA, (e.g., DPPC-rich gel phase) as a function of the DPPC mole fraction of the sample, χ_P,

$$FA \times x + (1 - FA) \times y = \chi_P, \quad \text{where } x < \chi_P < y. \tag{1}$$

Therefore, we can determine two-phase fraction values, FA_1 and FA_2, at their respective DPPC mole fractions, χ_{P1} and χ_{P2}, and can calculate:

$$x = \frac{\chi_{P1} \times (1 - FA_2) - \chi_{P2} \times (1 - FA_1)}{FA_1 \times (1 - FA_2) - FA_2 \times (1 - FA_1)}$$

$$y = \frac{\chi_{P1} \times FA_2 - \chi_{P2} \times FA_1}{FA_2 \times (1 - FA_1) - FA_1 \times (1 - FA_2)}. \tag{2}$$

The x and y values determine the phase coexistence boundary. When there are multiple data sets of $\{FA, \chi_P\}$, a vector plot of $\{FA\}$ versus $\{\chi_P\}$ should result in a straight line. The goodness of fit of a regression of this line shows the degree of consistency to classical two-phase equilibria. Furthermore, the intercept of the regression provides the error weighted estimate of the phase compositions, (x, y).

For DLPC and DPPC mixtures, GUV studies showed a classical coexistence region between a more disordered DLPC-rich phase and a more ordered DPPC-rich phase between DPPC molar fractions of 0.3 and 0.8 (Feigenson and Buboltz, 2001). When we analyzed the GUV images, we

corrected the spherical geometry pixel by pixel to convert the data into two-dimensional projections of the actual surface areas. We excluded a small edge region from the estimate to minimize associated conversion errors. For both AFM and GUV images, appropriate cutoff values were selected to differentiate between competing phases. We assumed that the relative area for each phase approximates the molar fraction of the phases (see Discussion for quantitative estimate). The deduced DLPC-rich fraction follows a straight line as required by the phase balance rule (Fig. 5). The intercepts of the regression lines yield ($x_{\text{DLPC-rich}}$, $y_{\text{DPPC-rich}}$) = (0.28, 0.87) (Fig. 5), where $x_{\text{DLPC-rich}}$ represents the mole fraction of DPPC in the DLPC-rich phase, and are consistent with the Feigenson and Buboltz (2001) interpretation. Near the center of the GUV phase coexistence region, our AFM phase balance measurements also follow a straight line (Fig. 5). This suggests that a phase structure similar to that described for GUVs also exists for mica-supported membranes. The corresponding intercepts yield ($x_{\text{DLPC-rich}}$, $y_{\text{DPPC-rich}}$) = (0.46, 0.89). The combined AFM data demonstrate that the phase boundaries shifted markedly along the zero cholesterol line.

DISCUSSION

Domain formation patterns

We observed spontaneous domain formations with mixtures of three lipid components and quantified the domain size distributions. Interestingly, the domains showed a flat, step-like structure with a height of 1.42 ± 0.24 nm for various mixture ratios. The factors that could cause these height differences include 1), carbon chain length differences (C16 in the case of DPPC versus C12 for DLPC); 2), tilt angle of the acyl chains; and 3), interdigitation between the two bilayer leaflets. The diameter of domains range from nanometer (25–50 nm) to submicrometer and up to micrometers. Larger domains were often found connected to the edge of the membranes patches. However, the majority of the nanometer scale domains occurred not only at the edge of the membrane, but also throughout the middle of DLPC-rich domains. This may be because 1), nanoscale domains are freer to move laterally in the membrane; 2), the domains fuse and/or move away from each other; and/or 3), they are kinetically trapped in a DLPC-rich phase. We did not observe any domain-like structures (lower height domains) in the higher DPPC-rich domains. If such domains exist, they must be very small and hidden by the presence of taller lipid molecules covering or blocking the AFM probe tip from detecting recessed domains. A further discussion of this domain pattern is embodied in the new phase diagram below.

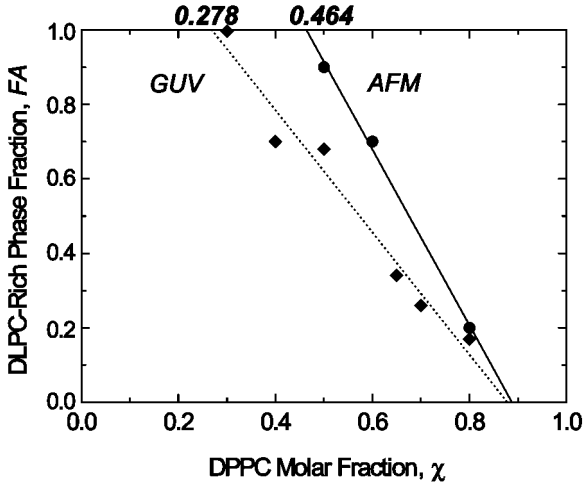

FIGURE 5 Phase balance analyses of membranes imaged as GUV by CFMand AFM. The DPPC molar fraction (χ_{DPPC}) and DLPC-rich phase area fraction (FA) are plotted. (♦) Areas obtained from GUV images after their 3-D areas were converted to 2-D projections. (●) Area fractions measured in AFM images. These plots were calculated as linear regressions and their x-axis intercepts at DLPC area fractions of 0 and 1 were considered as phase boundaries. We expect to see only a DLPC-rich phase at $\chi_{\text{DPPC}} \leq 0.28$ for GUV and $\chi_{\text{DPPC}} \leq 0.46$ by AFM. Similarly, only a DPPC-rich phase should be seen at $\chi_{\text{DPPC}} \geq 0.87$ for GUV and $\chi_{\text{DPPC}} \geq 0.89$ by AFM. The AFM-derived intercept at $FA = 1$ is shifted toward a higher χ_{DPPC} value; a much smaller shift is seen at $FA = 0$.

Proposed phase diagram

By collating AFM and CFM data sets, we constructed a new, three-dimensional phase diagram for supported lipid membranes (Fig. 6).

For the first part of the phase diagram, we consider the case of DLPC and DPPC mixtures without cholesterol. Our data show that both microscopic and nanoscopic domain sizes changed dependent upon relative lipid concentrations. A marked drop in nanoscopic domain size at $\chi_{\text{DPPC}} = 0.5$ along the $\chi_{\text{chol}} = 0$ isocline and morphologically different microscopic domains suggests that another phase boundary exists between $\chi_{\text{DPPC}} = 0.2$ and $\chi_{\text{DPPC}} = 0.5$. The nanoscopic domain sizes then gradually increase with increasing χ_{DPPC} up to $\chi_{\text{DPPC}} = 0.8$. We did not detect additional phase boundaries in this region (Fig. 4, *light green region*). However, according to the results of the phase boundary analysis shown in Fig. 5, phase boundaries must occur at approximately $\chi_{\text{DPPC}} = 0.46$, and 0.89. Compared with CFM data (Fig. 5) for GUVs, the phase boundary shift is larger in the DLPC-rich phase (0.28 → 0.46) than in the DPPC-rich phase (0.87 → 0.89) region. Fundamentally, our new data supplement and extend the previously reported GUV-based phase diagram; we also confirmed the miscibility of DPPC in a DLPC-rich phase, a miscibility gap at $0.46 \leq \chi_{\text{DPPC}} \leq 0.89$, and, finally, miscibility of DLPC in a DPPC-rich phase at $0.89 \leq \chi_{\text{DPPC}}$.

The phase boundary determination in Fig. 5 (using Eqs. 1 and 2) involves the following two approximations. First, the property that should be considered in this analysis with Eqs. 1 and 2 is the molar ratio of the two phases at first-order

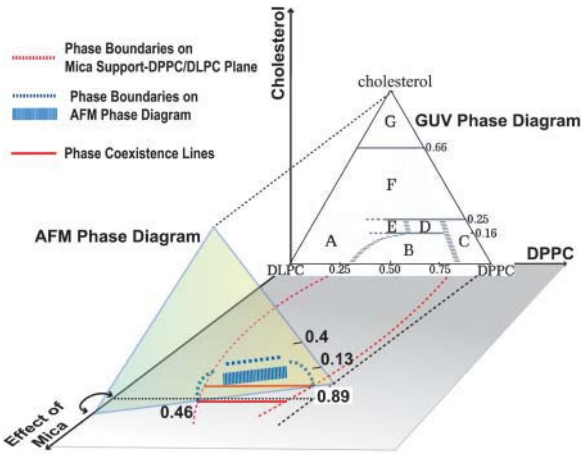

FIGURE 6 Three-Component phase diagram for a supported lipid bilayer. An AFM-derived phase diagram obtained using solid support is superimposed on a GUV-derived phase diagram. The AFM-derived phase diagram is rotated counter clockwise relative to the GUV-derived original phase diagram orientation due to substrate effects (*black dotted line*). A larger substrate effect was seen in the DLPC-rich phase than in the DPPC-rich phase. The AFM phase diagram also predicts two new phase boundary values ($\chi_{DPPC} = 0.45$ and 0.89) at $\chi_{chol} = 0$. Individual AFM-derived phase boundaries are connected to those on the GUV-derived phase diagram (*red dotted lines*). Two solid red lines show the coexistence of phases due to solid substrate effects. Blue lines are predicted phase boundaries and transition regions based on AFM data. The phase diagram for the supported membrane is based on the first bilayer in a monovalent buffer (5 mM PIPES, 200 mM KCl, and 1 mM EDTA, pH = 7.0) formed over mica support via extruded LUV adsorption.

coexistence. In both the AFM and CFM data, we determined the ratio of the membrane areas occupied by the two phases, FA, and used them in place of the molar ratio as an approximation. However, the molecular areas of saturated DLPC and DPPC are typically $\sim$0.53 nm^2 in their gel phase and $\sim$0.65 nm^2 in their fluid, liquid-crystalline phase (Marsh, 1990). The coexisting phases we observed at room temperature are mixtures at different composition ratios and may have similar molar area differences of $\delta \cong (0.65 - 0.53)/0.65 \cong 20\%$. To translate the membrane area fractions, FA, in Fig. 5 to molar fractions, $F\alpha$, we can deduce the shift to the leading order of δ as $F\alpha - FA \cong FA \times (FA - 1) \times \delta$. For $\delta \cong 20\%$, this shifts all the data points in Fig. 5 by less than 5%. Thus, this first approximation does not modify significantly our phase boundary determinations. As a second approximation, we note that our phase balance analyses assume that the DLPC-rich and the DPPC-rich phase areas change with total lipid composition whereas the nature of the two phases, such as their compositions, remains unchanged. With respect to the phase-diagram (Fig. 6), this requires that the coexistence lines at [chol] = 0.0 be horizontal. Because the actual coexistence lines may be tilted slightly for the supported membrane (as indicated in Fig. 6, and see below), our phase-boundary values may also be only a close approximation. In summary, the above estimates for the phase boundaries along the DLPC and DPPC mixtures line without cholesterol appear robust both for GUV membranes and supported bilayers.

For the second aspect of the phase diagram, in the presence of cholesterol, we estimate the phase boundaries from AFM imaging data along the DLPC/DPPC line for $\chi_{DPPC} = 0.6$ and 0.7 to be similar but not identical to those seen in the original GUV phase diagram (Fig. 6). The domain structures at $\chi_{chol} = 0.135$ observed by AFM (Fig. 3 *b*) are consistent with region D of the GUV phase diagram between $0.16 < \chi_{chol} < 0.25$, where nanoscopic phase separations were inferred to occur (Feigenson and Buboltz, 2001). Based on our data, phase boundaries on mica supported membranes should occur at two places, near $\chi_{chol} \cong 0.13$ and $\sim$0.3 (between $\chi_{chol} = 0.2$ and 0.4). However, the first phase boundary at $\chi_{chol} \cong 0.13$ would be diffuse because transitional microscopic domain sizes were observed by AFM for both $\chi_{DPPC} = 0.6$ (Fig. 3 *b*) and 0.7 (data not shown). Therefore, region D in the original diagram is shifted to lower cholesterol values and the phase transition may not be abrupt; a non-first-order transition or continuous transition may occur between regions B and D. In this transition region, a noticeable increase in nanoscopic domains size (Fig. 3 *b*) indicates that 1), DPPC-rich domains are less likely to coalesce; 2), smaller domains, if they exist, have an increased tendency to fuse; and/or 3), there are fewer nucleation sites that can precipitate phase transitions. Conversely, domain sizes between $\chi_{chol} =$ 0.189 and 0.40 have size differences of about $\sim$15 nm (data not shown) and we represent these and similar phenomena as a dotted line between $\chi_{chol} = 0.2$ and 0.4. The order and exact location of this phase boundary remains to be determined.

For the remainder of the phase diagram, we predict the existence of two-phase boundary paths connecting the GUV phase diagram and the AFM-modified phase diagram (Fig. 6, *red dotted lines*), and we depict a rotation of the entire phase-plane and a tilting of coexistence lines (Fig. 6, *solid red lines* on the mica-DPPC/DLPC plane). We denote the effect of mica as a representation of the interactions that modify the supported bilayers from the GUV membranes. In our AFM study, however, entropy suppression (see below) adds to the likelihood that a mica surface may shift the free-energy states in ways dependent upon the lipid mixture, as evident by the larger shift in the DLPC-rich phase, $\chi_{DPPC} = 0.28 \rightarrow 0.46$ for $\chi_{chol} = 0$. This has the effect of rotating the phase plane as well as tilting the coexistence lines. In GUVs, because other factors such as the ionic strength of the buffer are constant, the DLPC-rich/DPPC-rich phase coexistence line appeared along the DPPC/DLPC line for $\chi_{chol} = 0$. The tilt in the phase-coexistence lines for the supported bilayer explains why we observed a gradual increase in domain size in the coexistence region when $0.46 \leq \chi_{DPPC} \leq 0.89$ and $\chi_{chol} = 0$. When the composition of the lipid mixture changes along the line [chol] = 0, both the nature of the coexisting phases and the relative molar distribution of the two phases change. The apparent linearity of the data in our

phase balance analyses (Fig. 5) and the lack of dramatic changes in the nanoscopic domain characteristics (Table 1), however, suggest that the tilting in the phase diagram is probably small, as we assumed for the coexistence boundary estimation presented above.

Entropy suppression in supported membrane

The main thrust of our work was to estimate the effects of a supporting substrate on a ternary phase diagram. The primary factor affecting phase behavior equilibrium in GUVs is the relative concentrations of DPPC, DLPC, and cholesterol. The observed nanoscopic domain formations and marked shifts in phase boundaries depend on interactions the aggregate of which must be attractive between the membrane and the solid (mica) surface. The mica surface provides an extra stabilizing effect and suppresses movement of the lipid molecules both within and outside of the membrane plane (entropy suppression). Because the DLPC-rich phase is fluid-like and the DPPC-rich phase is gel-like, we expect a greater loss of entropy due to membrane undulations for the DLPC-rich phase than for the DPPC-rich phase. Thus, the free energy of the DLPC-rich phase is shifted to a higher value relative to that of the DPPC-rich phase. Therefore, this entropic effect causes the DLPC-rich phase to be less stable than the DPPC-rich phase. Other forces that can hold membranes to a mica support include an electrostatic force (Egawa and Furusawa, 1999), hydrophobic and hydration forces, and van der Waals attraction forces (Ederth et al., 1998; Muresan and Lee, 2001; Parsegian and Evans, 1996). It is difficult to discriminate between the two phases in a three-component system on the bases of these force contributions. Therefore, we propose that in this system entropy suppression is sufficient to cause the phase shift that we have observed. In fact, it has already been demonstrated that by AFM a phase transition temperature shift to a higher temperature occurs in a mica-supported dimyristoylphosphatidylcholine (DMPC) bilayer (Tokumasu et al., 2002). A similar effect was observed for a DPPC bilayer (data not shown). All the features depicted in Fig. 6 are consistent with the expectation that entropy suppression from reduced membrane undulations is larger for the fluid-like phase than for the gel-like phase.

Beyond the rationale for entropy suppression induced by flat mica substrates, we recognize the possible effects of partial membrane coverage and geometric constraints on membrane properties. With partial membrane coverage, we have membrane patch edges that may directly alter membrane/mica interactions near the membrane edges or indirectly alter the free energy contributions at the spatial scale of patch sizes that are typically a few micrometers in our membrane ensembles. It is interesting that the DPPC-rich phase and not the DLPC-rich phase prefers membrane edges as shown in Fig. 2, *a* and *c*, perhaps reflecting a combination of factors. It is possible that domains rich in DPPC with longer acyl chains prefer membrane edges where semi-micelle-like structures could theoretically form to cover hydrophobic chains, minimizing the thermodynamic energy state, and reduce bare substrate/patch line tension (May, 2000). Indeed, line tension is a useful concept for understanding domain shapes (e.g., Muresan and Lee, 2001) and is relevant to our observations.

For the direct substrate-edge interactions, the characteristic length scale is probably not greater than the size of the nanoscopic domains, i.e., ~40 nm. If that is the case, then, the relative area of the direct edge zones of our membrane patches can be estimated as,

$$\frac{W_N \times L_N}{A} \approx \frac{W_N \times 2\pi R}{\pi R^2} = \frac{W_N \times 2}{R}, \qquad (3)$$

where W_N is the diameter of the nanoscopic domain, L_N is the length of the bilayer edges, and A is the area of the membrane bilayer. Assuming $W_N = 40$ nm as the nanoscopic domain size and $R = 2.5$ μm as the radius of the membrane patch, we estimate that only 3.2% of the area is under the direct influence of membrane edge effects and substrate interactions. In addition, we propose that the edges and holes in the supported bilayer may have some indirect effects on membrane properties. In fact, similar membrane size limits and geometric constraints also play a role in the behavior of GUV membranes and are especially involved in lipid orientation/tilting orders (e.g., MacKintosh, 1994; MacKintosh and Lubensky, 1991). However, the supported bilayers in our experiments are often as large as our scan size of 5 μm. Therefore, nanoscopic domain size distributions per se should not depend on the size of the supported membranes we observed.

Our supported membranes were prepared in a monovalent ionic buffer, which is known to favor uniform and relatively weak membrane/mica attachments (Egawa and Furusawa, 1999). Membranes subjected to other environments may respond differently, which would affect the offset of the respective phase diagrams (cf. Fig. 6, in the mica support direction). The observed domain formation and phase diagram changes may be the consequence of different membrane-forming lipid mixtures interacting with a uniform support of the membrane along a rigid surface. Strong localized effects from the mica surface are probably not significant in this system because the quantity and appearance of the nanoscopic and microscopic domains are strongly dependent on the lipid mixture composition. In a previous study (Tokumasu et al., 2002), nonuniformities in local surface properties could induce a slight phase transition temperature shift within a single membrane, but were not strong enough to induce the generation of structural domains. What we have demonstrated here are the physical-chemical similarities and differences between a free vesicle system and a supported lipid bilayer that influence their lateral organization and membrane domain structure.

Biological implications and conclusion

In biological systems, cell membranes are often supported and interact with cytoskeletal proteins, neighboring membrane stacks, and extracellular matrices. In the case of a polarized membrane, apical and basolateral membranes interact differently with their immediate environments. For example, an apical membrane encounters extrinsic materials or agents, whereas basolateral membranes experience electrostatic repulsions/attractive forces and ionic screening effects mediated by intercellular fluids. These interactions affect native lipid phase behavior. Proteins, alcohol, and certain drugs can also alter membrane phase behavior and structure (Mou et al., 1994; Lasch et al., 1998; Hata et al., 2000). Cellular membranes are composed of a larger variety of lipids than the three-component system described here. Biological membrane heterogeneities, or membrane rafts, are functionally important, complex structures (Anderson and Jacobson, 2002; London and Brown, 2000). Nevertheless, it is useful to apply our AFM-derived phase diagram to supported cell membranes by substituting the mica-support axis with biologically relevant external agents and interactions. The direction and degree of phase diagram modifications will depend upon the net membrane charge, absolute interactive strength, membrane composition, and the degree of membrane confinement. The entropy suppression effects on lipid molecules by a solid support we report here are a reasonable first approximation of the phase behavior of native cell membranes.

Our direct observation and quantitation of nanoscopic domains together with a theoretical analysis provide detailed information on 1), domain formations of mixtures of DLPC, DPPC, and cholesterol; 2), the relationship between microscopic and nanoscopic domains; 3), the effect of a solid support on lipid phase behavior; and 4), some insights into the mechanisms behind these observations. The phase behavior and structural domain formation in an ionic environment detected by AFM approximates cell membrane behavior encountered in a native environment and points the way to an improved understanding of the physical chemical properties of cell membranes and their associated physiology.

We thank Dr. Horia Petrache at NIH for reading the manuscript and helpful comments, and the anonymous referees for stimulating debates especially on the effect of geometric constraints on membrane properties.

F.T. is a Japan Society for the Promotion of Science (JSPS) Research Fellow in Biomedical and Behavioral Research at National Institutes of Health, Bethesda, Maryland, USA. G.W.F. received support from National Science Foundation Grant MCB-0077630.

REFERENCES

Anderson, R. G. W., and K. Jacobson. 2002. A Role for Lipid Shells in Targeting Proteins to Caveolae, Rafts, and Other Lipid Domains. *Science*. 296:1821–1825.

Balgavy, P., M. Dubnickova, N. Kucerka, M. A. Kiselev, S. P. Yaradaikin, and D. Uhrikova. 2001. Bilayer thickness and lipid interface area in unilamellar extruded 1,2-diacylphosphatidylcholine liposomes: a small-angle neutron scattering study. *Biochim. Biophys. Acta*. 1512: 40–52.

Bedzyk, M. J., D. H. Bilderback, G. M. Bommarito, M. Caffrey, and J. S. Schildkraut. 1988. X-ray standing waves: a molecular yardstick for biological membranes. *Science*. 241:1788–1791.

Braet, F., C. Seynaeve, R. De Zanger, and E. Wisse. 1998. Imaging surface and submembranous structures with the atomic force microscope: a study on living cancer cells, fibroblasts and macrophages. *J. Microsc*. 190:328–338.

Brown, D. A., and E. London. 2000. Structure and function of sphingolipid- and cholesterol-rich membrane rafts. *J. Biol. Chem*. 275: 17221–17224.

Buboltz, J. T., and G. W. Feigenson. 1999. A novel strategy for the preparation of liposomes: rapid solvent exchange. *Biochim. Biophys. Acta*. 1417:232–245.

Bustamante, C., and D. Keller. 1995. Scanning Force Microscopy in Biology. *Physics Today*. 48:32–38.

Cevc, G., and D. Marsh. 1987. Phospholipid bilayers: physical principles and models. Wiley. New York.

Dietrich, C., L. A. Bagatolli, Z. N. Volovyk, N. L. Thompson, M. Levi, K. Jacobson, and E. Gratton. 2001. Lipid rafts reconstituted in model membranes. *Biophys. J*. 80:1417–1428.

Diociaiuti, M., F. Bordi, A. Motta, A. Carosi, A. Molinari, G. Arancia, and C. Coluzza. 2002. Aggregation of Gramicidin A in Phospholipid Langmuir-Blodgett Monolayers. *Biophys. J*. 82:3198–3206.

Dufrene, Y. F., T. Boland, J. W. Schneider, W. R. Barger, and G. U. Lee. 1998. Characterization of the physical properties of model biomembranes at the nanometer scale with the atomic force microscope. *Faraday Discuss*. 111:79–94.

Ederth, T., P. Claesson, and B. Liedberg. 1998. Self-assembled monolayers of alkanethiolates on thin gold films as substrates for surface force measurements. Long-range hydrophobic interactions and electrostatic double-layer interactions. *Langmuir*. 14:4782–4789.

Egawa, H., and K. Furusawa. 1999. Liposome adhesion on mica surface studied by atomic force microscopy. *Langmuir*. 15:1660–1666.

Feigenson, G. W., and J. T. Buboltz. 2001. Ternary phase diagram of dipalmitoyl-PC/dilauroyl-PC/cholesterol: nanoscopic domain formation driven by cholesterol. *Biophys. J*. 80:2775–2788.

Giocondi, M. C., V. Vie, E. Lesniewska, J. P. Goudonnet, and C. Le Grimellec. 2000. In situ imaging of detergent-resistant membranes by atomic force microscopy. *J. Struct. Biol*. 131:38–43.

Hata, T., H. Matsuki, and S. Kaneshina. 2000. Effect of local anesthetics on the bilayer membrane of dipalmitoylphosphatidylcholine: interdigitation of lipid bilayer and vesicle-micelle transition. *Biophys. Chem*. 87:25–36.

Henderson, E., P. G. Haydon, and D. S. Sakaguchi. 1992. Actin filament dynamics in living glial cells imaged by atomic force microscopy. *Science*. 257:1944–1946.

Hwang, J., L. K. Tamm, T. S. Ramalingam, E. Betzig, and M. Edidin. 1995. Nanoscale complexity of phospholipid monolayers investigated by near-field scanning optical microscopy. *Science*. 270:610–614.

Jin, A. J., D. Huster, K. Gawrisch, and R. Nossal. 1999. Light scattering characterization of extruded lipid vesicles. *Eur. Biophys. J*. 28: 187–199.

Kaasgaard, T., O. G. Mouritsen, and K. Jorgensen. 2002. Lipid domain formation and ligand-receptor distribution in lipid bilayer membranes investigated by atomic force microscopy. *FEBS Lett*. 515: 29–34.

Kingsley, P. B., and G. W. Feigenson. 1979. The synthesis of perdeuterated phospholipid: 1,2-dimyristoyl-sn-glycero-3-phosphocholine-d_{72}. *Chem. Phy. Lipids*. 24:135–147.

Koenig, B. W., S. Krueger, W. J. Orts, C. F. Majkrzak, N. F. Berk, J. V. Silverton, and K. Gawrisch. 1996. Neutron Reflectivity and Atomic Force Microscopy Studies of a Lipid Bilayer in Water Adsorbed to the Surface of a Silicon Single Crystal. *Langmuir*. 12:1343–1350.

Lang, T., D. Bruns, D. Wenzel, D. Riedel, P. Holroyd, C. Thiele, and R. Jahn. 2001. SNAREs are concentrated in cholesterol-dependent clusters that define docking and fusion sites for exocytosis. *EMBO J.* 20: 2202–2213.

Lasch, P., C. P. Schultz, and D. Naumann. 1998. The influence of poly-(L-lysine) and porin on the domain structure of mixed vesicles composed of lipopolysaccharide and phospholipid: an infrared spectroscopic study. *Biophys. J.* 75:840–852.

London, E., and D. A. Brown. 2000. Insolubility of lipids in triton X-100: physical origin and relationship to sphingolipid/cholesterol membrane domains (rafts). *Biochim. Biophys. Acta.* 1508:182–195.

MacKintosh, F. C. 1994. Mixed Fluid Bilayers—Effects of Confinement. *Phys. Rev. E.* 50:2891–2897.

MacKintosh, F. C., and T. C. Lubensky. 1991. Orientational Order, Topology, and Vesicle Shapes. *Phys. Rev. Lett.* 67:1169–1172.

Magonov, S. N., V. Elings, and M.-H. Whangbo. 1997. Phase imaging and stiffness in tapping-mode atomic force microscopy. *Sur. Sci. Lett.* 375:L385–L391.

Marsh, D. 1990. Handbook of Lipid Bilayers. CRC Press, Boca Raton.

May, S. 2000. A molecular model for the line tension of lipid membranes. *The European Physical Journal E.* 3:37–44.

Milhiet, P. E., C. Domec, M. C. Giocondi, N. Van Mau, F. Heitz, and C. Le Grimellec. 2001. Domain formation in models of the renal brush border membrane outer leaflet. *Biophys. J.* 81:547–555.

Mou, J., J. Yang, C. Huang, and Z. Shao. 1994. Alcohol induces interdigitated domains in unilamellar phosphatidylcholine bilayers. *Biochemistry.* 33:9981–9985.

Muller, D. J., J. B. Heymann, F. Oesterhelt, C. Moller, H. Gaub, G. Buldt, and A. Engel. 2000. Atomic force microscopy of native purple membrane. *Biochim. Biophys. Acta.* 1460:27–38.

Muresan, A. S., and K. Y. C. Lee. 2001. Shape evolution of lipid bilayer patches adsorbed on mica: An atomic force microscopy study. *J. Phys. Chem. B.* 105:852–855.

Nagao, E., and J. A. Dvorak. 1998. An integrated approach to the study of living cells by atomic force microscopy. *J. Microsc.* 191:8–19.

Nagle, J. F., and S. Tristram-Nagle. 2000. Lipid bilayer structure. *Curr. Opin. Struct. Biol.* 10:474–480.

Ono, A., and E. O. Freed. 2001. Plasma membrane rafts play a critical role in HIV-1 assembly and release. *Proc. Natl. Acad. Sci. USA.* 98:13925–13930.

Parsegian, V. A., and E. A. Evans. 1996. Long and short range intermolecular and intercolloidal forces. *Curr. Opin. Colloid Interf. Sci.* 1:53–60.

Pencer, J., G. F. White, and F. R. Hallett. 2001. Osmotically induced shape changes of large unilamellar vesicles measured by dynamic light scattering. *Biophys. J.* 81:2716–2728.

Sheets, E. D., D. Holowka, and B. Baird. 1999. Critical role for cholesterol in Lyn-mediated tyrosine phosphorylation of FcepsilonRI and their association with detergent-resistant membranes. *J. Cell Biol.* 145:877–887.

Sikes, H. D., and D. K. Schwartz. 1997. Two-dimensional melting of an anisotropic crystal observed at the molecular level. *Science.* 278: 1604–1607.

Simons, K., and E. Ikonen. 1997. Functional rafts in cell membranes. *Nature.* 387:569–572.

Stefanova, I., V. Horejsi, I. J. Ansotegui, W. Knapp, and H. Stockinger. 1991. GPI-anchored cell-surface molecules complexed to protein tyrosine kinases. *Science.* 254:1016–1019.

Swihart, A. H., J. M. Mikrut, J. B. Ketterson, and R. C. Macdonald. 2001. Atomic force microscopy of the erythrocyte membrane skeleton. *J. Microsc.* 204:212–225.

Takeyasu, K., H. Omote, S. Nettikadan, F. Tokumasu, A. Iwamoto-Kihara, and M. Futai. 1996. Molecular imaging of Escherichia coli F0F1-ATPase in reconstituted membranes using atomic force microscopy. *FEBS Lett.* 392:110–113.

Tokumasu, F., A. J. Jin, and J. A. Dvorak. 2002. Lipid membrane phase behaviour elucidated in real time by controlled environment atomic force microscopy. *J. Electron Microsc. (Tokyo).* 51:1–9.

Ushiki, T., J. Hitomi, T. Umemoto, S. Yamamoto, H. Kanazawa, and M. Shigeno. 1999. Imaging of living cultured cells of an epithelial nature by atomic force microscopy. *Arch. Histol. Cytol.* 62:47–55.

Yuan, C., and L. J. Johnston. 2001. Atomic force microscopy studies of ganglioside GM1 domains in phosphatidylcholine and phosphatidylcholine/cholesterol bilayers. *Biophys. J.* 81:1059–1069.